

Nonorientability-induced \mathcal{PT} phase transition in ladder latticesJung-Wan Ryu,¹ Nojoon Myoung,² Martina Hentschel,³ and Hee Chul Park^{1,*}¹*Center for Theoretical Physics of Complex Systems, Institute for Basic Science, Daejeon 34051, Republic of Korea*²*Department of Physics Education, Chosun University, Gwangju 61452, Republic of Korea*³*Institute of Physics, Faculty of Natural Sciences, Technische Universität Chemnitz, Reichenhainer Strasse 70, 09126 Chemnitz, Germany*

(Received 4 February 2020; revised 17 March 2021; accepted 23 March 2021; published 7 April 2021)

We study parity-time (\mathcal{PT}) phase transitions in the energy spectra of ladder lattices caused by the interplay between nonorientability and non-Hermitian \mathcal{PT} symmetry. The energy spectra show level crossings in circular ladder lattices with increasing on-site energy gain-loss because of the orientability of a normal strip. However, the energy levels show \mathcal{PT} phase transitions instead of the avoided level crossings of a Hermitian situation in \mathcal{PT} -symmetric Möbius ladder lattices due to the nonorientability of a Möbius strip. The latter effectively presents a perturbation that would cause avoided level crossing in a Hermitian situation, but leads, in the presence of \mathcal{PT} symmetry, to locked real energy parts and conjugate values of the imaginary parts. In order to understand the level crossings of \mathcal{PT} -symmetric phases, we generalize the rotational transformation using a complex rotation angle. We also study the modification of resonant tunneling induced by a sharply twisted interface in \mathcal{PT} -symmetric ladder lattices. Finally, we find that perfect transmissions at the zero energy are recovered at the exceptional points of the \mathcal{PT} -symmetric system due to the self-orthogonal states.

DOI: [10.1103/PhysRevA.103.042207](https://doi.org/10.1103/PhysRevA.103.042207)**I. INTRODUCTION**

Non-Hermitian physics has attracted considerable attention not only as an important alternative to the Hermitian formalism of quantum mechanics in open systems with energy gain and loss [1] but also for applications in various optical and photonic systems [2–7]. In a non-Hermitian system, the eigenvalues are complex and the eigenstates form a biorthogonal set. The complex eigenvalues have a clear physical meaning: the real and imaginary parts represent the eigenenergy of a state and its decay rate, respectively.

The Möbius strip, discovered independently by Möbius and Listing in 1858, is a continuous one-sided surface formed by rotating one end of a rectangular strip through 180 deg and attaching it to the other end [8,9]. This marvelous structure with only one side and only one boundary is the epitome of a topologically nontrivial system and shows curious properties due to its nonorientability. A surface in Euclidean space is orientable if a two-dimensional figure cannot be moved around the surface and back to where it started so that it looks like its own mirror image [10,11]. Otherwise, the surface is nonorientable. Besides fundamental studies on topology, the nonorientability of Möbius strips has enabled their use in many applications in various fields [12–15].

The real-space Möbius strip is therefore a fascinating system both for mathematicians and physicists. Physics in particular allows one to realize Möbius strip topologies in various contexts beyond real space. For example, an exceptional point (EP), which is a degenerate point of eigenenergies in a non-Hermitian system, generates this structure in

parametric space because of the square root branch property of the singular point [16,17]. Such a Möbius strip of eigenenergies generated in parameter space has been reported in microwave experiments [18,19], optical microcavities [20], and a chaotic exciton-polariton billiard [21]. One of the interesting phenomena originating from the nontrivial topology of non-Hermitian systems is parity-time (\mathcal{PT}) symmetry, which exhibits a spontaneous symmetry-breaking transition from an unbroken \mathcal{PT} symmetric phase to a broken phase via EPs [22]. \mathcal{PT} symmetry is protected in non-Hermitian systems with a balance of energy gain and loss represented by the commutation relation $[H, \mathcal{PT}] = 0$, where H is a Hamiltonian. Many \mathcal{PT} -symmetric systems have been explored in several fields, including optics [2,3,23–27], electronic circuits [28], atomic physics [29], and magnetic metamaterials [30].

While the nontrivial Möbius topology in real space has been widely applied in chemistry [13,14] and biology [15], there have been only a few related studies in physics [31–33]. Most of these studies were particularly focused on the topological properties of quantum states in Hermitian systems [31,32]. In this paper we study how the nonorientability of a Möbius strip, corresponding to topological nontriviality, generates and affects the \mathcal{PT} phase transitions in tight-binding models by comparing circular and Möbius ladder lattices as the simplest models in real space. Additionally, corresponding resonances and antiresonances appearing in quantum transport in quasi-one-dimensional lattices are also studied and compared to the energy spectra in circular and Möbius ladder lattices.

This paper is organized as follows. In Sec. II we introduce the two systems, circular and Möbius ladder lattices, and then review their characteristics. In Sec. III we study eigenenergy evolution as a function of on-site potential in

*hcpark@ibs.re.kr

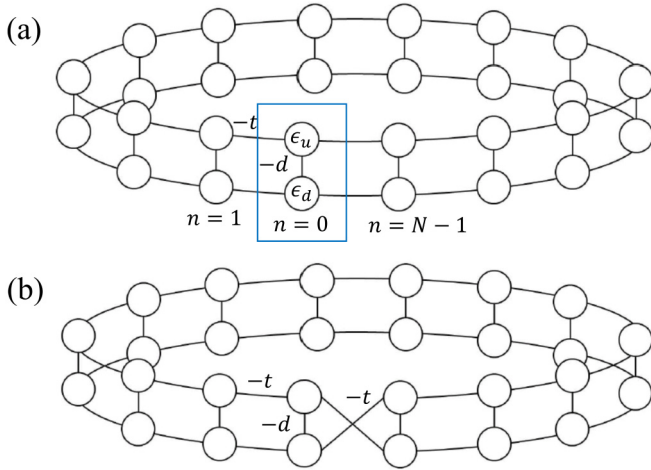


FIG. 1. (a) A circular ladder lattice (CLL) and (b) a Möbius ladder lattice (MLL). The blue box represents the unit cell of the CLL, which has two sites with intra-unit cell hopping strength d and inter-unit cell hopping strength t .

\mathcal{PT} -symmetric cases, and in Sec. IV we consider quantum transport in \mathcal{PT} -symmetric ladder and twisted-ladder lattices corresponding to \mathcal{PT} -symmetric circular and Möbius ladder lattices, respectively. Section V summarizes our results.

II. SYSTEMS: CIRCULAR AND MÖBIUS LADDER LATTICES

Figure 1(a) depicts a circular ladder lattice (CLL). The on-site potentials of the upper and lower sites are ϵ_u and ϵ_d , respectively, while the intra- and inter-unit cell hopping strengths are d and t , respectively. The Hamiltonian of an infinite ladder lattice can be expressed on the basis of Pauli matrix $\boldsymbol{\sigma} = (\sigma_x, \sigma_z)$ and k -independent vector field $\mathbf{h} = (-d, \delta/2 + i\gamma/2)$ as

$$H(k) = \mathbf{h} \cdot \boldsymbol{\sigma} + h_0(k)\sigma_0, \quad (1)$$

where the extra term $h_0(k) = -t \cos k$ and σ_0 is an identity matrix. δ and γ will be used to describe antisymmetric on-site potentials when we consider Hermitian and \mathcal{PT} -symmetric situations. The eigenvalues of the Hamiltonian are

$$\epsilon_{\pm} = \pm |\mathbf{h}| + h_0(k) = -2t \cos k \pm \sqrt{d^2 + \left(\frac{\delta}{2} + i\frac{\gamma}{2}\right)^2}, \quad (2)$$

which are complex with $\epsilon = \epsilon_r + i\epsilon_i$. If $d = 0$, a CLL can be divided into two circular lattices with hopping strength t .

Next we consider the Möbius ladder lattice (MLL) shown in Fig. 1(b) [34]. On-site potentials and inter- and intra-unit cell hopping strengths are the same as those in the CLL; the only difference is that one pair of parallel hoppings changes into cross hoppings. In this paper we model the Möbius strip with an abrupt change in the hopping parameters and leave the study of a smooth parameter change to a subsequent work. If $d = 0$, the MLL can be considered as one circular lattice with two times the length of the MLL, which reflects the intrinsic properties of a Möbius strip.

We consider a CLL with symmetric on-site potential, i.e., $\epsilon_u = \epsilon_d = 0$. The energy bands of the CLL are separated into

two subbands in which states are equally distributed to upper and lower lattices with odd and even parities, respectively. As d and t increase, the distance between the two bands and the bandwidths increase, respectively. Using a periodic boundary condition, the eigenvalues of the Hamiltonian of a CLL with N sites are

$$\epsilon_{\pm} = -2t \cos \frac{2n\pi}{N} \pm d \quad (n = 1, \dots, N), \quad (3)$$

where ϵ_{\pm} are the eigenvalues of the corresponding eigenstates with odd and even parities, i.e., $u_u(x) = -u_d(x)$ and $u_u(x) = u_d(x)$, respectively.

Eigenenergies in the MLL can be obtained by replacing the boundary condition for a CLL with that for an MLL. As a result, the eigenvalues of the Hamiltonian of an MLL with N sites are

$$\begin{aligned} \epsilon_- &= -2t \cos \frac{2n\pi}{N} - d \quad \text{for even parity,} \\ \epsilon_+ &= -2t \cos \frac{(2n-1)\pi}{N} + d \quad \text{for odd parity,} \end{aligned} \quad (4)$$

where $n = 1, \dots, N$. The Bloch wave vectors and corresponding eigenenergies are the same as those in the CLL in the case of even-parity eigenstates but different in the case of odd-parity eigenstates. The upper and lower sites exhibit opposite signs of amplitudes in the case of odd-parity eigenstates, which correspond to opposite orientations, while the sites have the same signs of amplitudes (meaning no orientations) in the case of even-parity eigenstates. Consequently, for the even-parity case, there is no effect of breaking orientation in the MLL since there is no orientation even in the CLL. This changes when odd-parity states are considered. It is noted that the symmetry of the unit cell plays an important role in obtaining eigenenergies.

The difference between normal rings and Möbius ring structures according to the parity of the eigenstates has previously been studied [35]. It has also been found that the difference in eigenenergies in the case of odd-parity in a Möbius ring structure is related to the noninteger azimuthal mode indices in three-dimensional optical Möbius strip cavities [33]. In this case, the polarization of light induces an orientation, such as opposite signs of the amplitudes of the odd-parity eigenstates. In the next section we study the \mathcal{PT} phase transitions of complex eigenenergies in \mathcal{PT} -symmetric cases.

III. ENERGY SPECTRA IN \mathcal{PT} -SYMMETRIC CIRCULAR AND MÖBIUS LADDER LATTICES

We consider \mathcal{PT} -symmetric systems that can possess entirely real eigenvalues, which is a crucial factor in the transport problems of the next section. A \mathcal{PT} -symmetric CLL with balanced gain and loss is introduced with antisymmetric imaginary on-site potentials in Eq. (1), i.e., $\epsilon_u = -\epsilon_d = i\gamma/2$. Here the system parameters are $d = t = 1$. The non-Hermitian CLL with \mathcal{PT} symmetry exhibits complex-conjugate paired energy bands in the \mathcal{PT} -broken phase and real eigenenergies otherwise.

Figures 2(a) and 2(c) show a \mathcal{PT} phase transition between unbroken and broken \mathcal{PT} -symmetric phases possessing real

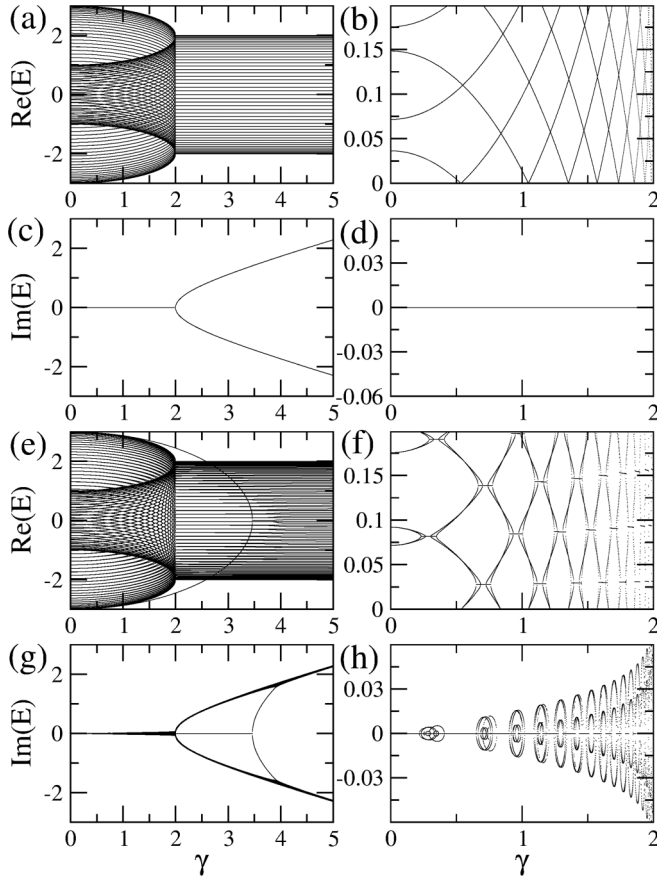


FIG. 2. (a) Real and (c) imaginary parts of the eigenenergies as a function of γ in a \mathcal{PT} -symmetric CLL with 100 unit cells when $d = t = 1$. (b) Real and (d) imaginary parts of the selected eigenenergies. (e) Real and (g) imaginary parts of the eigenenergies as a function of γ in a \mathcal{PT} -symmetric MLL with 100 unit cells when $d = t = 1$. (f) Real and (h) imaginary parts of the selected eigenenergies. See also Figs. 3 and 4 below.

and complex conjugate eigenenergies, respectively. As γ increases in the range of $0 < \gamma < \gamma_b$, pairs of real energies approach each other to ultimately merge at a corresponding \mathcal{PT} phase transition point $\gamma_b = 2d$. After the transition at $\gamma = \gamma_b$, degenerate energies split into two complex conjugate energies, and the absolute values of the imaginary parts increase as γ increases. The two bands are separable, and thus there is no band touching except for the case of the EPs, $\gamma = \gamma_b$, in the \mathcal{PT} -symmetric CLL. In the case of the unbroken phase, the real energy bands are separated with their imaginary parts being zero, and thus their states are equally distributed to the upper and lower lattices in spite of the \mathcal{PT} -symmetric on-site potential [see Fig. 3(b)]. In the case of the broken phase, the complex energy bands are separated, while their real parts are the same. The eigenstates belonging to the positive and negative imaginary energy are not equally distributed to the upper and lower circular lattices, respectively. It is noted that \mathcal{PT} -symmetric on-site potential in a \mathcal{PT} -symmetric CLL makes the real parts of the energies attractive, as shown in Fig. 2(a), while antisymmetric real on-site potential in a CLL makes the real energies repulsive [36].

Considering only the unbroken region of $0 < \gamma < \gamma_b$, the evolution of the eigenenergies shows energy level crossings as

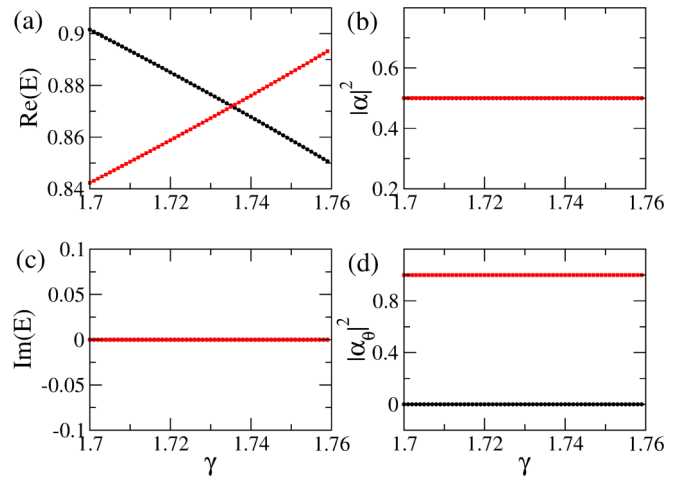


FIG. 3. (a) Real and (c) imaginary parts of the eigenenergies in a \mathcal{PT} -symmetric CLL showing level crossings of real eigenenergies of a non-Hermitian system in the \mathcal{PT} -unbroken phase. (b) $|\alpha|^2$ of two pairs of degenerate eigenstates and (d) $|\alpha_\theta|^2$ of two pairs of degenerate eigenstates.

γ increases, as seen in Fig. 2(b), because of the orthogonality of the two separated energy bands. The eigenstates of the Hamiltonian are given by

$$|\psi\rangle = \alpha|\psi_a\rangle + \beta|\psi_b\rangle, \quad (5)$$

where $|\psi_a\rangle = (1, 0)^T$ and $|\psi_b\rangle = (0, 1)^T$. The corresponding eigenstates with unbroken phases are equally distributed to the upper and lower lattices, i.e., $|\alpha|^2 = |\beta|^2 = 0.5$, as shown in Fig. 3(b). Using unitary matrix U , the Hamiltonian changes into a diagonalized Hamiltonian H_θ as

$$UHU^\dagger = H_\theta, \quad (6)$$

where

$$U = \begin{pmatrix} \cos \theta & -\sin \theta \\ \sin \theta & \cos \theta \end{pmatrix}. \quad (7)$$

From the diagonalized condition of H_θ , the general rotating angle θ is derived as

$$\theta = \frac{1}{2} \operatorname{arccot} \left(\frac{i\gamma}{2d} \right). \quad (8)$$

Rotation angle θ is complex in a \mathcal{PT} -symmetric CLL but real in a Hermitian CLL with antisymmetric real on-site potential. Writing complex angle $\theta = \theta_r + i\theta_i$ for a general non-Hermitian system, the states can be transformed through basis transformation with

$$\begin{aligned} \frac{\delta + i\gamma}{2d} &= \cot 2\theta \\ &= \frac{\cos 2\theta_r \sin 2\theta_i - i \sinh 2\theta_i \cosh 2\theta_i}{\sin^2 2\theta_r \cosh^2 2\theta_i + \cos^2 2\theta_r \sinh^2 2\theta_i}, \end{aligned} \quad (9)$$

which has two conditions from real and imaginary equations. For the Hermitian case, the rotating angle can be derived from this result in cases of $\theta_i = 0$. Here \mathcal{PT} symmetry gives a constraint in that the real part of the equation is zero and there are two regimes, \mathcal{PT} -unbroken and broken phases, regardless of the fact that we only have an interest in the unbroken

phases because of energy level crossings and \mathcal{PT} -symmetric transitions. In the region of bulk states with unbroken phases when $\gamma < \gamma_b$ in a \mathcal{PT} -symmetric CLL, the transformation is satisfied by $\frac{\gamma}{2d} = \tanh(2\theta_i)$ with $\theta_r = \frac{\pi}{4} + n\frac{\pi}{2}$ ($n \in \mathbb{Z}$).

Using the rotation of the basis states, the eigenstates $|\psi_\theta\rangle$ are given by

$$|\psi_\theta\rangle = \alpha_\theta |\psi_a^\theta\rangle + \beta_\theta |\psi_b^\theta\rangle, \quad (10)$$

where

$$|\psi_a^\theta\rangle = U |\psi_a\rangle, \quad (11)$$

$$|\psi_b^\theta\rangle = U |\psi_b\rangle. \quad (12)$$

Applying rotation to the states, $|\alpha_\theta|^2$ and $|\beta_\theta|^2$ are changed into 0.0 or 1.0 as shown in Fig. 3(d), while both $|\alpha|^2$ and $|\beta|^2$ are equal to 0.5 as shown in Fig. 3(b). On the other hand, in the region of bulk broken phases when $\gamma > \gamma_b$, the transformation is satisfied by $\frac{\gamma}{2d} = \coth(2\theta_i)$ with $\theta_r = n\frac{\pi}{2}$ ($n \in \mathbb{Z}$).

Figures 2(e)–2(h) show evolutions of the eigenenergies in a \mathcal{PT} -symmetric MLL with gain and loss on the upper and lower lattices, respectively, as γ increases. The difference between the \mathcal{PT} -symmetric CLL and the \mathcal{PT} -symmetric MLL lies in the existence of \mathcal{PT} phase transitions in the unbroken regime of the latter when $\gamma < \gamma_b$ and a pair of emergent interface states with a \mathcal{PT} phase transition taking place at $\gamma = 2\sqrt{3}$ by complex energy inversion appears [37]. As shown in Fig. 2(f), the \mathcal{PT} phase transition in the \mathcal{PT} -symmetric MLL takes place at a pair of EPs originating from degenerate points in the \mathcal{PT} -symmetric CLL, which are diabolic points (not EPs) [Fig. 2(b)]. The two EPs are developed with increasing \mathcal{PT} -symmetric potential, where a pair of real energies merge at one EP and repel at the other, while a pair of imaginary energies repel at one EP and merge at the other. Through this process, the quantum states show \mathcal{PT} phase transitions from unbroken to broken and back to unbroken states again. This effect is caused by the finite size and discrete lattice of the system in our MLL with an abrupt parameter change, of which the lengths between paired EPs of the nonorientability induced \mathcal{PT} phase transitions decrease as the system size increases. We can clearly see the \mathcal{PT} phase transitions through measurements of quantum transport in the lattice systems in the following section.

While there are many energy crossings in the unbroken region when $\gamma < \gamma_b$ in the case of a \mathcal{PT} -symmetric CLL, many pairs of \mathcal{PT} phase transitions appear in a \mathcal{PT} -symmetric MLL. Figure 4 shows strong and weak \mathcal{PT} phase transitions and also that a Hermitian degenerate point splits into a pair of non-Hermitian degenerate points, or EPs, due to the non-Hermiticity of this case. The strong or weak \mathcal{PT} phase transition means that the region of broken states is wider or narrower. The eigenstates have unbroken phases, of which eigenenergies are real, before the \mathcal{PT} phase transitions, where $|\alpha|^2 = |\beta|^2 = 0.5$ as shown in Fig. 4(b). In the region, $|\alpha_\theta|^2$ and $|\beta_\theta|^2$ decrease from 1.0 or increase from 0.0. After the \mathcal{PT} phase transition, i.e., in the broken region, $|\alpha|^2$ and $|\beta|^2$ do not equal 0.5 but are rather closely related to the imaginary parts of the eigenenergies. In the broken region, $|\alpha_\theta|^2$ and $|\beta_\theta|^2$ are equal to 0.5.

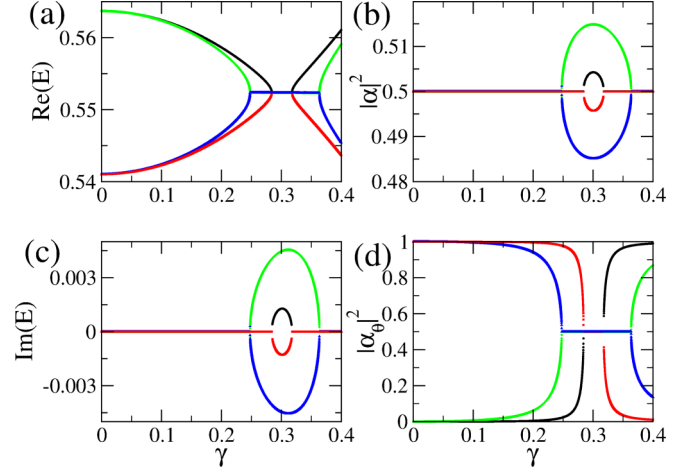


FIG. 4. Same as Fig. 3 but for the MLL. (a) Real and (c) imaginary parts of the eigenenergies in a \mathcal{PT} -symmetric MLL. (b) $|\alpha|^2$ of four eigenstates and (d) $|\alpha_\theta|^2$ of four eigenstates. The formation of a pair of EPs sandwiching a region of broken \mathcal{PT} phase is clearly visible.

Finally, we can understand the emergence of a pair of EPs in a \mathcal{PT} -symmetric MLL instead of a level crossing in a \mathcal{PT} -symmetric CLL as follows. Cross hopping at a point of the lattice with asymmetric on-site potentials causes the degeneracies to be lifted through the geometric perturbation, which transforms the CLL into an MLL. In the case of a Hermitian Hamiltonian with real asymmetric on-site potential, it is known that level crossings at the degeneracy points in the real energy spectra change into avoided level crossings due to perturbation breaking the symmetries. \mathcal{PT} symmetry, however, requires that the degenerate points with real energies of unbroken \mathcal{PT} phases in the CLL are lifted into complex conjugated energies of broken \mathcal{PT} phases in the MLL. For the non-Hermitian case without \mathcal{PT} symmetry, the degenerate points are separated into complex energies—that is, \mathcal{PT} symmetry guarantees that the degeneracy in unbroken \mathcal{PT} phases is lifted into broken \mathcal{PT} phases when introducing a \mathcal{PT} -symmetric perturbation. The eigenstates of the MLL near the level crossing points are dictated by the broken \mathcal{PT} -symmetric states due to the \mathcal{PT} phase transition, while the MLL eigenstates far from the level crossing points converge to the unbroken \mathcal{PT} -symmetric states of the CLL. By varying the non-Hermitian parameter across the level crossing points, the unbroken phases evolve into broken phases via an EP and then back into unbroken phases via another EP. As a result, the degeneracy point in the CLL changes into a pair of exceptional points in the MLL by perturbation under \mathcal{PT} symmetry.

IV. TRANSPORT IN CORRESPONDING LADDER LATTICES

In this section we discuss quantum transport in ladder and twisted-ladder lattices exhibiting energy-level crossings and \mathcal{PT} phase transitions like as in the CLL and MLL. Quantum transport provides important signatures of defects embedded in the system as scattering states. The properties of the defects are represented by phase shifts or interference in the

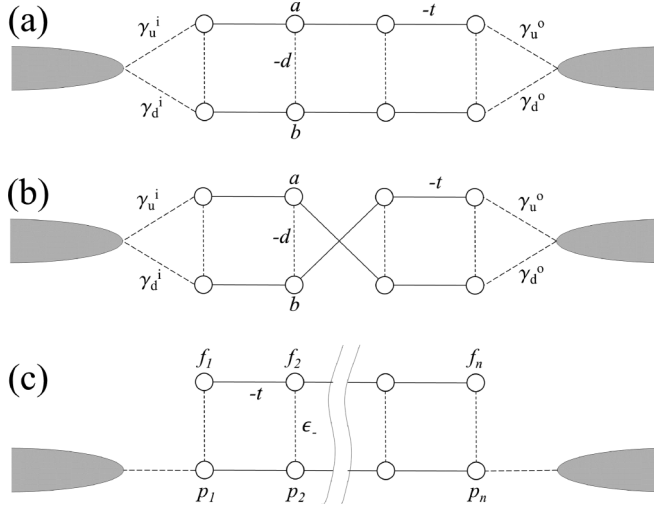


FIG. 5. (a) A ladder lattice with two leads. The unit cell has two sites, a and b , with hopping strengths d (dashed lines) and t (solid lines) between the sites. The coupling strength between sites and leads is $\gamma_u^{i(o)}$ (long-dashed lines). (b) A twisted-ladder lattice with two leads. (c) Detangled Fano lattices from a ladder lattice with symmetric contacts corresponding to (a). The hopping strength between f_n and p_n is $\epsilon_- = (\epsilon_u - \epsilon_d)/2$.

transmission probability. A reconfiguration of the quantum states and corresponding quantum transport in \mathcal{PT} -symmetric lattices has previously been demonstrated in quasi-one-dimensional lattices [38,39], where the quantum states can be controlled by a \mathcal{PT} -symmetric potential. In the broken phase, the group velocity has been found to be a complex number, of which the imaginary part is reflected in the suppression of the transmission due to the attenuation of the evanescent modes. As a result, quantum transport in the lattice with normal metallic leads is measured only in the unbroken \mathcal{PT} phases in the energy band (i.e., real spectra), not in the broken \mathcal{PT} phases. Here, in addition, the geometrically nontrivial lattice with non-Hermitian \mathcal{PT} symmetry exhibits novel transport signatures.

Let us consider quantum transport in a ladder lattice with antisymmetric imaginary on-site potential, i.e., $\epsilon_u = -\epsilon_d = i\gamma/2$. The system under study is composed of a ladder lattice with N unit cells, as shown in Fig. 5(a), with two leads connected to the left and right end unit cells. The Hamiltonian of this system is given by

$$H = H_{\text{LL}} + H_{\text{lead}} + H_{\text{coupling}}, \quad (13)$$

where H_{LL} , H_{lead} , and H_{coupling} describe the ladder lattice, leads, and coupling between the lattice and leads, respectively, and are given by

$$H_{\text{LL}} = \sum_{i=1}^N H_0 d_i^\dagger d_i + \sum_{i=1}^{N-1} (H_1 d_{i+1}^\dagger d_i + \text{H.c.}), \quad (14)$$

$$H_{\text{lead}} = -\frac{V_0}{2} \sum_{j \neq 0} (c_{j+1}^\dagger c_j + \text{H.c.}), \quad (15)$$

$$H_{\text{coupling}} = -G^i d_1^\dagger c_{-1} - G^o d_N^\dagger c_1 + \text{H.c.}, \quad (16)$$

where

$$H_0 = \begin{pmatrix} \epsilon_u & -d \\ -d & \epsilon_d \end{pmatrix}, \quad H_1 = \begin{pmatrix} -t & 0 \\ 0 & -t \end{pmatrix}, \quad (17)$$

and d_j^\dagger (d_j) and c_j^\dagger (c_j) are particle creation (annihilation) operators for the lattice and leads, respectively. $V_0/2$ is the hopping strength in the leads and $G^{i(o)}$ describes the coupling between the lattice and the left (right) lead. Considering a twisted-ladder lattice with two leads as in Fig. 5(b), Eq. (14) has to be changed into

$$H_{\text{LL}} = \sum_{i=1}^N H_0 d_i^\dagger d_i + \sum_{i \neq N/2, i=1}^{N-1} (H_1 d_{i+1}^\dagger d_i + \text{H.c.}) + H_1' (d_{N/2+1}^\dagger d_{N/2} + \text{H.c.}), \quad (18)$$

where

$$H_1' = \begin{pmatrix} 0 & -t \\ -t & 0 \end{pmatrix}, \quad (19)$$

which induces cross coupling such as in the MLL.

We construct ladder and twisted ladder lattices of 100 unit cells with symmetric contacts, that is, $\gamma_u^i = \gamma_d^i = \gamma_u^o = \gamma_d^o = \gamma_0$, and $t = d = 1$. Throughout this work we set $\gamma_0 = 1$. Figures 6(a) and 6(d) show the eigenenergy spectra of the ladder and twisted-ladder lattices, respectively. Using the above Hamiltonian, transmission probability $T = |t|^2$ can be obtained as a function of γ and energy E , as shown in Figs. 6(b) and 6(e) corresponding to each lattice (see the Appendix). It is noted that $|r|^2 + |t|^2 = 1$ in \mathcal{PT} -symmetric systems where $|r|^2$ and $|t|^2$ are the reflection and transmission probabilities, respectively, whereas $|r|^2 + |t|^2 \neq 1$ in non-Hermitian systems that do not preserve \mathcal{PT} symmetry.

The paired eigenenergies of the ladder lattices are attracted under \mathcal{PT} symmetry while the energies are repelled in the Hermitian system. For the ladder lattice, the unbroken \mathcal{PT} phase shows level crossings of real eigenenergies, and the broken \mathcal{PT} phase, $\gamma > \gamma_b$, maintains constant real eigenenergies as shown in Fig. 6(a). For the twisted-ladder lattice, on the other hand, the energy spectra show \mathcal{PT} phase transitions at multiple pairs of EPs corresponding to the energy level crossings in the unbroken region in the \mathcal{PT} -symmetric ladder lattice, as shown in Fig. 6(d). It is from the features that distinguish the twisted ladder from the ladder lattices that the level crossings and \mathcal{PT} phase transitions are developed as a function of on-site potential $i\gamma$.

The level crossings and \mathcal{PT} phase transitions are reflected by resonant and antiresonant peaks through Breit-Wigner and Fano resonances by means of quantum transport in both \mathcal{PT} symmetric ladder lattices, as shown in Figs. 6(b) and 6(c) and Figs. 6(e) and 6(f). Transmission can be well explained by the energy spectra in both \mathcal{PT} -symmetric ladder and twisted-ladder lattices; the transmission peaks trace the energy spectra of the systems. The attached leads, however, perturb the system and modify the self-energy as a non-Hermitian parameter so that the symmetry of the system is broken. This modification lifts the degeneracy points, which is reflected by a transmission suppression at these points. For the simple ladder lattice, the resonance peaks at zero energy are suppressed with increasing non-Hermitian parameter γ , even in the resonant

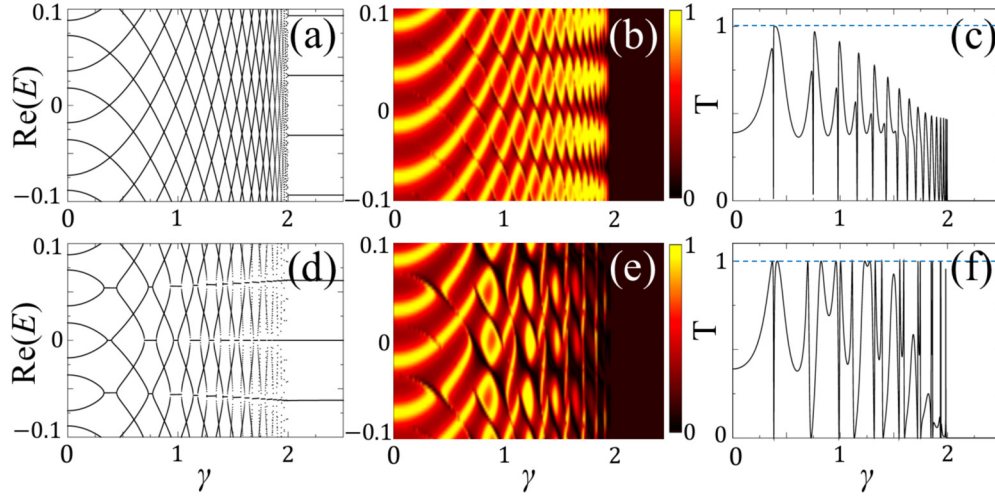


FIG. 6. (a) Eigenenergies as a function of imaginary antisymmetric on-site potential γ in a ladder lattice with 100 unit cells. (b) Transmission probability for the ladder lattice in which both a and b sites of the end unit cells are connected to the input and output leads. Yellow, red, and black colors denote the highest, middle, and lowest transmission probabilities, respectively. (c) Transmission probability as a function of γ when $\text{Re}(E) = 0$. (d) Eigenenergies as a function of γ in a ladder lattice with 100 unit cells and one twisted hopping. (e) Transmission probability for the twisted-ladder lattice in which both a and b sites of the end unit cells are connected to the input and output leads. (f) Transmission probability as a function of γ when $\text{Re}(E) = 0$. The dark regions in (e) appear larger than in (b) reflecting the presence of evanescent modes corresponding to imaginary eigenenergies in the broken \mathcal{PT} phase.

condition. A leakage of transmissions is reflected but current flux is still conserved, similar to the Hermitian systems.

For the twisted-ladder lattice, as aforementioned, the twisted boundary, causing nonorientability-induced perturbation, introduces a \mathcal{PT} phase transition at the crossed levels, which can be captured through resonant transmission. The twisted boundary reveals perfect resonance, since the attracted energies coalesce at the EP characterized by self-orthogonality. Transmission probability at these islands of broken \mathcal{PT} symmetry in the $\gamma < \gamma_b$ region is suppressed due to the presence of imaginary parts in the eigenenergies, cf. Fig. 6(e). Otherwise the transmission itself is perfect and reaches values of 1 even for increasing non-Hermitian parameter γ , see Fig. 6(f). This finding, that nonorientability reveals perfect transmission at zero energy through the \mathcal{PT} phase transition, is notable.

In order to understand the antiresonant states, let us consider the amplitude equations for a ladder lattice. The equations of the n th unit cell in a ladder lattice can be written as

$$E \mathbf{v}_n = \left(\frac{i\gamma}{2} \sigma_z - d \sigma_x \right) \mathbf{v}_n - t \sigma_0 (\mathbf{v}_{n-1} + \mathbf{v}_{n+1}), \quad (20)$$

where $\mathbf{v}_n = (a_n, b_n)$ is amplitude vector of the n th unit cell. Applying Eq. (7) to these equations, we obtain amplitude equations of rotated states, $\mathbf{g}_n = (f_n, p_n) = U(\theta) \mathbf{v}_n$, as follows:

$$E f_n = [(i\gamma/2) \cos 2\theta + d \sin 2\theta] f_n - t(f_{n-1} + f_{n+1}) + \mathcal{F}(\theta) p_n, \quad (21)$$

$$E p_n = [-(i\gamma/2) \cos 2\theta - d \sin 2\theta] p_n - t(p_{n-1} + p_{n+1}) + \mathcal{F}(\theta) f_n, \quad (22)$$

where θ is real and $\mathcal{F}(\theta) = [(i\gamma/2) \sin 2\theta - d \cos 2\theta]$ is a coupling term for the rotated equations that gives a detangled condition, Eq. (8), when this term is zero. The condition provides that the states are completely separated into two orthogonal states, f_n and p_n , while exhibiting energy crossings. Here the orthogonal basis is associated with the symmetry of the leads, which is helpful for understanding the measurement process. When the rotation angle is $\theta = \pi/4$, we get

$$E \mathbf{g}_n = \left(-d \sigma_z + \frac{i\gamma}{2} \sigma_x \right) \mathbf{g}_n - t \sigma_0 (\mathbf{g}_{n-1} + \mathbf{g}_{n+1}), \quad (23)$$

where the components of \mathbf{g}_n , $f_n = (a_n - b_n)/\sqrt{2}$ and $p_n = (a_n + b_n)/\sqrt{2}$, are antisymmetric and symmetric configurations, respectively. For the symmetric contacts with leads as shown in Fig. 5(c), p_n and f_n states result in resonance and antiresonance in transmission probability as a function of incoming energy and on-site potential, respectively, in Fig. 6. If we use an asymmetric contact, e.g., $\gamma_u^i = \gamma_u^o = 0$ and $\gamma_d^i = \gamma_d^o = \gamma_0$, both lattices with on-site potentials f_n and p_n result in resonances, with no antiresonance.

There is a crucial difference between Hermitian and non-Hermitian \mathcal{PT} -symmetric systems, namely whether the coupling between f_n and g_n in Eq. (23) is real or imaginary according to the system possessing real mass or \mathcal{PT} -symmetric mass. This imaginary coupling drives the attraction between the real parts of the paired energy bands and then shows a \mathcal{PT} phase transition. The transition is at a collective EP in both \mathcal{PT} -symmetric lattices at $\gamma = \gamma_b$ in Figs. 6(a) and 6(d). While the transmission probability shows resonant features of the bulk states in unbroken \mathcal{PT} phases, $\gamma < \gamma_b$, the transmission probability is completely suppressed in the broken phase, $\gamma > \gamma_b$, due to the lack of resonant energy in the real energy space, as shown in Figs. 6(b) and 6(e). The real eigenenergies of the unbroken \mathcal{PT} phases correspond to propagating modes, while the complex eigenenergies of the broken \mathcal{PT} phases are reflected in evanescent modes. As a result, in the broken \mathcal{PT}

- Observation of \mathcal{PT} -Symmetry Breaking in Complex Optical Potentials, *Phys. Rev. Lett.* **103**, 093902 (2009).
- [3] C. E. Rüter, K. G. Makris, R. El-Ganainy, D. N. Christodoulides, M. Segev, and D. Kip, Observation of parity-time symmetry in optics, *Nature Phys.* **6**, 192 (2010).
- [4] M. Liertzer, L. Ge, A. Cerjan, A. D. Stone, H. E. Türeci, and S. Rotter, Pump-Induced Exceptional Points in Lasers, *Phys. Rev. Lett.* **108**, 173901 (2012).
- [5] M. Brandstetter, M. Liertzer, C. Deutsch, P. Klang, J. Schöberl, H. E. Türeci, G. Strasser, K. Unterrainer, and S. Rotter, Reversing the pump dependence of a laser at an exceptional point, *Nat. Commun.* **5**, 4034 (2014).
- [6] H. Hodaei, A. U. Hassan, S. Wittek, H. Garcia-Gracia, R. El-Ganainy, D. N. Christodoulides, and M. Khajavikhan, Enhanced sensitivity at higher-order exceptional points, *Nature (London)* **548**, 187 (2017).
- [7] W. Chen, S. Kaya Özdemir, G. Zhao, J. Wiersig, and L. Yang, Exceptional points enhance sensing in an optical microcavity, *Nature (London)* **548**, 192 (2017).
- [8] A. F. Möbius, Über die bestimmung des inhaltes eines polyeders (On the determination of the volume of a polyhedron), *Ber. Verh. Sächs. Ges. Wiss.* **17**, 31 (1865); *Gesammelte Werke, Band II* (Collected Works, vol. II) (Hirzel, Leipzig, 1886).
- [9] J. B. Listing, Der Census räumlicher Complexe, oder Verallgemeinerung des Euler'schen Satzes von den Polyädern, *Abh. Königl. Ges. Wiss. Göttingen* **10**, 97 (1862).
- [10] M. Spivak, *Calculus on Manifolds: A Modern Approach to Classical Theorems of Advanced Calculus* (HarperCollins, New York, 1965).
- [11] A. Hatcher, *Algebraic Topology* (Cambridge University Press, Cambridge, 2001).
- [12] C. A. Pickover, *The Möbius Strip: Dr. August Möbius's Marvelous Band in Mathematics, Games, Literature, Art, Technology, and Cosmology* (Thunder's Mouth, New York, 2006).
- [13] D. M. Walba, R. M. Richards, and R. C. Haltiwanger, Total synthesis of the first molecular Möbius strip, *J. Am. Chem. Soc.* **104**, 3219 (1982).
- [14] G. Gil-Ramírez, D. A. Leigh, and A. J. Stephens, Catenanes: Fifty years of molecular links, *Angew. Chem.* **54**, 6110 (2015).
- [15] D. Han, S. Pal, Y. Liu, and H. Yan, Folding and cutting DNA into reconfigurable topological nanostructures, *Nat. Nanotechnol.* **5**, 712 (2010).
- [16] T. Kato, *Perturbation Theory of Linear Operators* (Springer, Berlin, 1996).
- [17] W. D. Heiss, The physics of exceptional points, *J. Phys. A* **45**, 444016 (2012).
- [18] C. Dembowski, H.-D. Gräf, H. L. Harney, A. Heine, W. D. Heiss, H. Rehfeld, and A. Richter, Experimental Observation of the Topological Structure of Exceptional Points, *Phys. Rev. Lett.* **86**, 787 (2001).
- [19] C. Dembowski, B. Dietz, H.-D. Gräf, H. L. Harney, A. Heine, W. D. Heiss, and A. Richter, Observation of a Chiral State in a Microwave Cavity, *Phys. Rev. Lett.* **90**, 034101 (2003).
- [20] S.-B. Lee, J. Yang, S. Moon, S.-Y. Lee, J.-B. Shim, S. W. Kim, J.-H. Lee, and K. An, Observation of an Exceptional Point in a Chaotic Optical Microcavity, *Phys. Rev. Lett.* **103**, 134101 (2009).
- [21] T. Gao, E. Estrecho, K. Y. Bliokh, T. C. H. Liew, M. D. Fraser, S. Brodbeck, M. Kamp, C. Schneider, S. Höfling, Y. Yamamoto, F. Nori, Y. S. Kivshar, A. G. Truscott, R. G. Dall, and E. A. Ostrovskaya, Observation of non-Hermitian degeneracies in a chaotic exciton-polariton billiard, *Nature (London)* **526**, 554 (2015).
- [22] C. M. Bender and S. Boettcher, Real Spectra in Non-Hermitian Hamiltonians Having \mathcal{PT} Symmetry, *Phys. Rev. Lett.* **80**, 5243 (1998).
- [23] R. El-Ganainy, K. G. Makris, D. N. Christodoulides, and Z. H. Musslimani, Theory of coupled optical \mathcal{PT} -symmetric structures, *Opt. Lett.* **32**, 2632 (2007).
- [24] Z. H. Musslimani, K. G. Makris, R. El-Ganainy, and D. N. Christodoulides, Optical Solitons in \mathcal{PT} Periodic Potentials, *Phys. Rev. Lett.* **100**, 030402 (2008).
- [25] K. G. Makris, R. El-Ganainy, D. N. Christodoulides, and Z. H. Musslimani, Beam Dynamics in \mathcal{PT} Symmetric Optical Lattices, *Phys. Rev. Lett.* **100**, 103904 (2008).
- [26] S. Klaiman, U. Günther, and N. Moiseyev, Visualization of Branch Points in \mathcal{PT} -Symmetric Waveguides, *Phys. Rev. Lett.* **101**, 080402 (2008).
- [27] A. Regensburger, C. Bersch, M. A. Miri, G. Onishchukov, D. N. Christodoulides, and U. Peschel, Parity-time synthetic photonic lattices, *Nature (London)* **488**, 167 (2012).
- [28] J. Schindler, A. Li, M. C. Zheng, F. M. Ellis, and T. Kottos, Experimental study of active LRC circuits with \mathcal{PT} symmetries, *Phys. Rev. A* **84**, 040101(R) (2011).
- [29] Y. N. Joglekar, D. Scott, M. Babbey, and A. Saxena, Robust and fragile \mathcal{PT} -symmetric phases in a tight-binding chain, *Phys. Rev. A* **82**, 030103(R) (2010).
- [30] N. Lazarides and G. P. Tsironis, Gain-Driven Discrete Breathers in \mathcal{PT} -Symmetric Nonlinear Metamaterials, *Phys. Rev. Lett.* **110**, 053901 (2013).
- [31] N. Zhao, H. Dong, S. Yang, and C. P. Sun, Observable topological effects in molecular devices with Möbius topology, *Phys. Rev. B* **79**, 125440 (2009).
- [32] Z. L. Guo, Z. R. Gong, H. Dong, and C. P. Sun, Möbius graphene strip as a topological insulator, *Phys. Rev. B* **80**, 195310 (2009).
- [33] J. Kreissmann and M. Hentschel, The optical Möbius strip cavity: Tailoring geometric phases and far fields, *Europhys. Lett.* **121**, 24001 (2018).
- [34] R. K. Guy and F. Harary, On the Möbius ladders, *Canadian Math. Bull.* **10**, 493 (1967).
- [35] Z. Li and L. R. Ram-Mohan, Quantum mechanics on a Möbius ring: Energy levels, symmetry, optical transitions, and level splitting in a magnetic field, *Phys. Rev. B* **85**, 195438 (2012).
- [36] J.-W. Ryu, N. Myoung, and H. C. Park, Antiresonance induced by symmetry-broken contacts in quasi-one-dimensional lattices, *Phys. Rev. B* **96**, 125421 (2017).
- [37] J.-W. Ryu, N. Myoung, A. Go, S. Woo, S.-J. Choi, and H. C. Park, Emergent localized states at the interface of a twofold \mathcal{PT} -symmetric lattice, *Phys. Rev. Research* **2**, 033149 (2020).
- [38] J.-W. Ryu, N. Myoung, and H. C. Park, Reconfiguration of quantum states in \mathcal{PT} -symmetric quasi-one-dimensional lattices, *Sci. Rep.* **7**, 8746 (2017).
- [39] H. C. Park, N. Myoung, and J.-W. Ryu, Quantum transport and non-Hermiticity on flat-band lattices, *J. Low Temp. Phys.* **191**, 49 (2018).